INTERNATIONAL JOURNAL OF AUTOMOTIVE AND MECHANICAL ENGINEERING (IJAME)
ISSN: 2229-8649 e-ISSN: 2180-1606
VOL. 19, ISSUE 3, 10002 – 10013
DOI: https://doi.org/10.15282/ijame.19.3.2022.12.0772

ORIGINAL ARTICLE

Motion Planning and Tracking Trajectory of an Autonomous Emergency Braking Pedestrian (AEB-P) System Based on Different Brake Pad Friction Coefficients on Dry Road Surface

Z. Abdullah[1], P.M. Heerwan[1,2*], M.A. Zakaria[3], M.I. Ishak[4], M.A. Shahrom[1] and B. Kujunni[3]

[1]Faculty of Mechanical and Automotive Engineering Technology, Universiti Malaysia Pahang, 26600 Pahang, Malaysia
[2]Automotive Engineering Center (AEC), Universiti Malaysia Pahang, 26600 Pahang, Malaysia
[3]Faculty of Manufacturing and Mechatronic Engineering and Technology, Universiti Malaysia Pahang, 26600 Pahang, Malaysia
[4]College of Engineering, Universiti Malaysia Pahang, 26600 Pahang, Malaysia

ABSTRACT – Accidents between vehicles and pedestrians usually occur when a pedestrian is crossing the road. An Autonomous Emergency Braking Pedestrian (AEB-P) is introduced to prevent collisions between vehicles and pedestrians. However, the performance of an AEB-P will be reduced when the brake pad is worn out on a dry road. In this study, the motion planning, namely Vehicle Conditional Artificial Potential Field (VC-APF), including a warning signal and emergency brake phase that generate the vehicle's deceleration, is proposed to analyze the effect of brake pad on the AEB-P performance. Then, the vehicle's deceleration is tracked by the tracking trajectory, where the PI controller is adapted to provide the optimum braking force. The function of PI control is to ensure the vehicle's deceleration is approaching the desired deceleration. The performance of the proposed method has been simulated on the dry road surface with different brake pad coefficients; 0.4, 0.35, and 0.24. The simulation results show that the vehicle manages to stop colliding with a pedestrian on the dry road surface at the minimum safety distance range of 2.7-2.9 meters.

ARTICLE HISTORY
Received: 26th Mar 2022
Revised: 26th Sept 2022
Accepted: 7th Oct 2022
Published: 11th Oct 2022

KEYWORDS
Autonomous emergency braking;
Artificial potential field;
Motion planning;
Tracking tarjectory;
Vehicle safety

INTRODUCTION

Advanced Driver Assistance Systems (ADAS) are enacted to protect road users in these circumstances. As a merger of numerous sophisticated systems, ADAS includes Adaptive Cruise Control (ACC), Autonomous Emergency Braking (AEB), Anti-lock Braking System (ABS), and many more [1, 2]. Although ADAS can prevent a collision, pedestrian-vehicle collisions are viewed as the most deliberate type of accident since they yield a high fatality rate. There were almost 316,000 cases of road disaster in the ASEAN Region, which was transcribed to a disaster rate of 17.0 per 100 000 population [1]. Meanwhile, in Malaysia, pedestrian fatalities registered roughly 500 deaths each year. The data continued to show that fatal road traffic crashes among the elderly (60 years old) are on the increase, climbing from 24.4 % in 2006 to 44.2 % in 2013 [3]. In terms of incident conditions, the statistics indicate that straight roads have the greatest number of pedestrian fatalities, followed by junction-type roads [3]. Frontal collisions are the most common form of accident in Malaysia, according to data from the Malaysian Institute of Road Safety Research (MIROS) [1]. Usually, an accident occurs because of the driver's incompetence to act in time [4].

AEB can prevent accidents by determining potential threats before the incident [5]. At low speeds, an AEB system has been found to be effective, reducing collisions by 35 % to 41% [6]. At speeds less than or equal to 50 km/h, crashes and injury events are reduced by 54–57% [6], but at speeds of 60–70 km/h, only 35–42% of collision is mitigated, respectively. Only 12–25 percent of the risk is avoided when the host vehicle reaches speeds of 80 km/h or greater [7].

The architecture of an AEB system consists of three essential elements: threat assessment strategies, motion planning, and tracking trajectory [8]. When involving the presence of the pedestrian as an obstacle, AEB is known as Autonomous Emergency Braking Pedestrian (AEB-P). Another pivotal aspect of the AEB-P system of an autonomous vehicle is its ability to calculate prior risk incidents and provide a possible replanned path in a hazardous situation. The motion planning system will receive the information fed by the pedestrian prediction motion system acting as a threat assessment that re-evaluates the vehicle's ongoing trajectory. After the threat assessment identifies the hazard and risk, an overriding system, namely motion planning, will replan the current trajectory to overcome the obstacle [9]. The potential-field-based method is one of the well-known path-planning approaches because of its simplicity in concept and application.

In [10], the author proposed the Artificial Potential Field (APF) approach, in which the robot movements as a result of the summation of attractive and repulsive forces in its environment. The attractive force [10] is the force that pulls the robot toward its destination, whereas the repulsive force [10] is the force that pulls the robot away from an obstacle. However, a team of researchers recently tried to improve a conventional algorithm by adding dynamic boundaries as well as environmental boundaries into the algorithm [11] and [12]. As a result, this method assures that the vehicle can no

*CORRESPONDING AUTHOR | P.M. Heerwan | ✉ mheerwan@ump.edu.my

longer be trapped in local minima situations. Finally, the researcher managed to provide an optimized replanned trajectory by manipulating the Potential Field's formulation [13].

The vehicle will then pursue the reassessment trajectory using a tracking trajectory [8]. As collisions in the real world commonly comprise high-speed moving vehicles; thus a decisive choice of each strategy is vital to ensure a timely AEB-P execution. The Proportional Integrative Derivative (PID) controller [14] is one of the traditional control systems that can be utilized to govern the trajectory. It is frequently utilized in commercial robotics, as well as in automotive and industrial applications. This controller's implementation is straightforward and yields acceptable results [15, 16].

Although AEB-P can prevent collision, the performance of AEB-P will be reduced if the brake fade phenomenon is occurred due to several factors, such as the brake pad being worn out. The term "brake fade" refers to the deterioration of braking performance at high temperatures. The deterioration of the binder phase, i.e. the pad material's phenolic resin, is the primary cause of this phenomenon. On a mesoscopic scale, the resin had degraded to the point of releasing [17]. As a result, these activities significantly increased the contact patch release rate, resulting in a decrease in the brake pad friction coefficient [17]. This event occurred as a result of the braking system overheating, which led to an increase in brake power loss. This is because the brake pad's surface must operate at a constant high temperature and uniform coefficient of friction throughout the braking process. The braking system's dissipation capability and heat storage must be considered in order to minimize brake fade caused by thermal overload during a single stop or several stops under high speed or high load circumstances [18]. Brake fading is also initiated by the braking pattern [18]. The researcher in [19] stated that the average friction coefficient is in the range of 0.35 to 0.38, 0.39 to 0.43, and 0.16 to 0.24, respectively, corresponding to tiredness test temperatures of the brake pad at low, medium, and high thermal levels of 100-150 °C, 200-250 °C, and 300-350 °C. When the vehicle brakes at low speed, more severe braking, and suffers severe emergency braking, the tiredness test of the brake pad is comparable in low, medium, and high temperatures. [19].

In this paper, the combination of Vehicle Conditional Artificial Potential Field (VC-APF) path planner with PI controller to get a feasible deceleration of the vehicle during the presence of pedestrian is proposed. The main objective of this paper is to analyze the motion planning and control performance of an AEB-P system. The AEB-P system performance is analyzed on the dry road surface as its brake disc friction coefficient varies from 0.4, 0.35 and 0.24. The system is simulated using MATLAB Simulink.

NUMERICAL ANALYSIS

Figure 1 shows the architecture of the proposed method, AEB-P, with vehicle conditional artificial potential field (VC-APF). This system consists of several modules, namely, pedestrian prediction motion, motion planning and decision-making, and vehicle dynamics control. Each module is explained in the following sub-topic. In this presence, Advanced Driver Assistance Systems (ADAS) are created to protect road user.

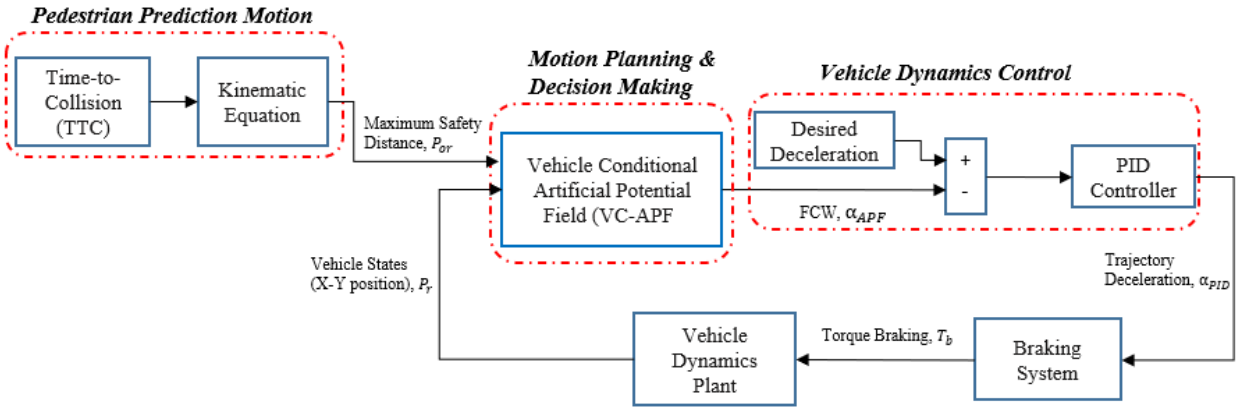

Figure 1. Architecture of an AEB-P system.

Analysis Vehicle Model

The sedan car, namely Proton Persona, is used as an analysis vehicle model in this study. Figure 2 shows the analysis vehicle model, while Table 1 shows the specifications of the vehicle [20].

Figure 2. Vehicle model.

Table 1. The specification of the analysis vehicle model.

Details	Symbol	Value	SI unit
Mass (Kerb Weight)	m	1330	kg
Center of gravity (c.g) length towards frontal part	l_f	1.107	m
Center of gravity (c.g) length towards rear part	l_r	1.643	m
Height of center gravity	h	0.479	m
Effective radius of the tire	r_{eff}	0.393	m

Since this study focuses on longitudinal motion, the vehicle model is designed based on a two degree of freedom (DoF). Figure 3 shows the forces acting on the vehicle while braking on the road.

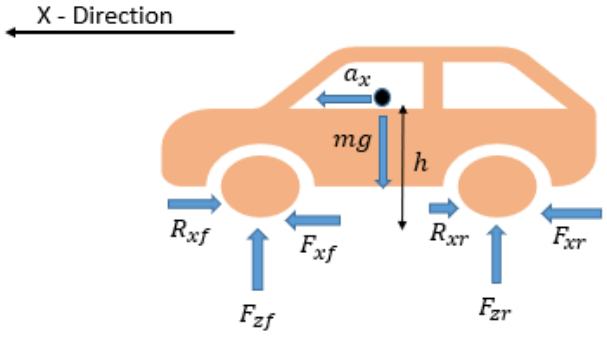

Figure 3. Forces acting on the vehicle model.

By neglecting the drag force, the vehicle dynamic equation of motion on the longitudinal axis can be written as in Eq. (1).

$$ma_x = F_{xf} + F_{xr} - R_x - D_a V_x^2 \tag{1}$$

where m is a vehicle mass, a_x is an acceleration/deceleration on the longitudinal axis, F_{xfr}, F_{xfl}, F_{xrr} and F_{xrl} is a longitudinal force at each tire. The nonlinear tire model, namely Dugoff tire model is used to determine the longitudinal force at each tire, and it is expressed as in Eq. (2).

$$F_x = C_\sigma \frac{\sigma_x}{1+\sigma_x} f(\lambda) \tag{2}$$

where C_σ is the longitudinal tire stiffness, σ_x is the slip ratio, while function, $f(\lambda)$ and the variable, λ are expressed as in Eq. (3) and Eq. (4).

$$f(\lambda) = \begin{cases} (2-\lambda)\lambda, & \lambda < 1 \\ 1 \quad , & \lambda \geq 1 \end{cases} \tag{3}$$

$$\lambda = \frac{\mu F_z (1+\sigma_x)}{2[(C_\sigma \sigma_x)^2 + (C_a \tan(a))^2]^{1/2}} \tag{4}$$

From Eq. (4), μ is tire-road adhesive friction, F_z is a dynamic load at each tire and β is a tire side slip angle. Considering β is zero during braking, Eq. (4) only influences the μ and F_z. Eq. (5) shows the equation of μ where k is a road coefficient, and its value depends on the road surface. For the dry surface, k is set as 0.9.

$$\mu_{brk} = -1.15k\,\{e^{-35\sigma_x} - e^{-0.35\sigma_x}\} \tag{5}$$

The longitudinal slip ratio during braking is defined in Eq. (6).

$$\sigma_x = \frac{r_{eff}\,\omega_w - V_x}{V_x} \tag{6}$$

where, r_{eff} is the effective radius of the tire, V_x is the longitudinal velocity, and ω_w acts as a rotational velocity of the tire. Rearranging Eq. (1), the equation for acceleration, a_x of host vehicle considering the tire-road friction coefficient is expressed as in Eq. (7).

$$a_x = \frac{F_{xfr} + F_{xfl} + F_{xrr} + F_{xrl}}{m} \tag{7}$$

AUTONOMOUS EMERGENCY BRAKING PEDESTRIAN (AEB-P)

AEB-P is a system that helps the vehicle avoid a collision by executing an emergency braking during the appearance of the pedestrian. Assuming a pedestrian is crossing a road, as in Figure 4., the trajectory route of the vehicle is planned to use the vehicle conditional APF (VC-APF) path planner. The vehicle's initial separation headway from the collision region is set to 90 metres in the simulation. The vehicle and pedestrian are both considered to be travelling at 64 km/h and 4.32 km/h, respectively. The distance x1 indicates a safety margin as pedestrians enter the roadside, and ×2 represents a safety margin as pedestrians exit the roadside. Both safety margins are set to 0.75 metres.

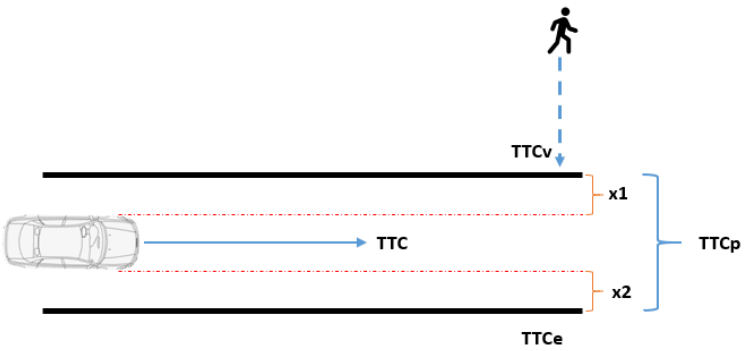

Figure 4. Illustration of VC-APF while a pedestrian is crossing a road.

Pedestrian Prediction Motion

In the AEB-P system, a pedestrian prediction motion will determine the position of the pedestrian as well as the vehicle by using time-to-collision (TTC). TTC is the time for the vehicle and pedestrian to enter the collision area. TTC is calculated by deriving the equation of the kinematic model when the obstacle appears in front of the vehicle as the vehicle is approaching it [21, 22].

$$|p| = \begin{cases} -vt & , \quad a = 0 \\ -vt + \frac{1}{2}at^2 & , \quad a \neq 0 \end{cases} \tag{8}$$

From the kinematic equation in Eq. (8), the velocity of the host vehicle is symbolized as *v,* while the deceleration of the host vehicle is symbolized as a. The time taken for the host vehicle to reach at a certain distance is symbolized as t, while the distance travelled by the host vehicle is represented as p. The time to collision (TTC) can be taken by rearranging the equation of the kinematic model as shown in Eq. (9).

$$TTC = \begin{cases} \frac{-v \pm \sqrt{v^2 + 2pa}}{a}, & v \geq 0 \; and \; a < 0 \end{cases} \tag{9}$$

By referring to the architecture of AEB-P in Figure 1, the AEB-P system is linked to TTC in the pedestrian prediction motion module to measure the maximum safety distance between the vehicle and the pedestrian. The theory of pedestrian prediction motion is illustrated in Figure 4., which consists of TTC, TTCv, TTCe and TTCp. TTCv is the time when a pedestrian collides with a road barrier, whereas TTCe is the time when a pedestrian flees the collision zone and enters a safe zone. TTCp is the time it takes for a pedestrian to safely cross the road from point TTCv to point TTCe. The collision will occur when the algorithm of the system meets the following condition [23]:

$$TTCv \leq TTC \leq TTCe \; \& \; TTCp \leq TTCe \tag{10}$$

If the vehicle and pedestrian is predicted to be in the collision area, the TTC value will fetch the kinematic equation to determine the maximum safety distance, ρ_{or} for emergency braking in the motion planning and decision making.

Maximum safety distance, ρ_{or} is also derived from the kinematic equation as shown in Eq. (11). Each variable in ρ_{or} such as d_0, v_c and a_{max} stands for critical safety distance, which is 2 m, current velocity, and maximum deceleration of the vehicle, respectively.

$$\rho_{or} = d_0 + (v_c \times TTC) + \frac{{v_c}^2}{2a_{max}} \tag{11}$$

where, ρ_{or} represents the safe distance while driving as the value is frequently changes depends on vehicles velocity and maximum deceleration of the vehicle.

Motion Planning and Decision Making

Motion planning considers the presence of a pedestrian in the environment using an artificial potential field (APF) to calculate the desired longitudinal motion of the vehicle, such as vehicle deceleration. Then, the APF is modified by including the phase of the vehicle during travel such as no signal, warning signal and full brake [22]. In this study, the Vehicle Conditional Artificial Potential Field (VC-APF) is used where it is influenced by the vehicle condition, which is the distance between the vehicle and obstacle. The shorter the distance between the vehicle and the obstacle, the greater the repulsive force generated at the impediment's centre [12]. Equation (12), (13) and (14) show the full braking, warning signal and free states of the AEB-P system, as illustrated in Figure 5. Equation (15) shows the deceleration produced by the VC-APF path planner.

$$F_{rep}(X) = \frac{1}{2}n\left(\frac{1}{\rho_r} - \frac{1}{\rho_{or}}\right)\frac{1}{\rho_r{}^2} \quad if,\ \rho_r \leq \rho_{or} \tag{12}$$

$$F_{rep}(X) = warning\ signal \quad if,\ \rho_{or} \leq \rho_r \leq \rho_{or} + 1.5 \tag{13}$$

$$F_{rep}(X) = no\ signal \quad if,\ \rho_r \geq \rho_{or} + 1.5 \tag{14}$$

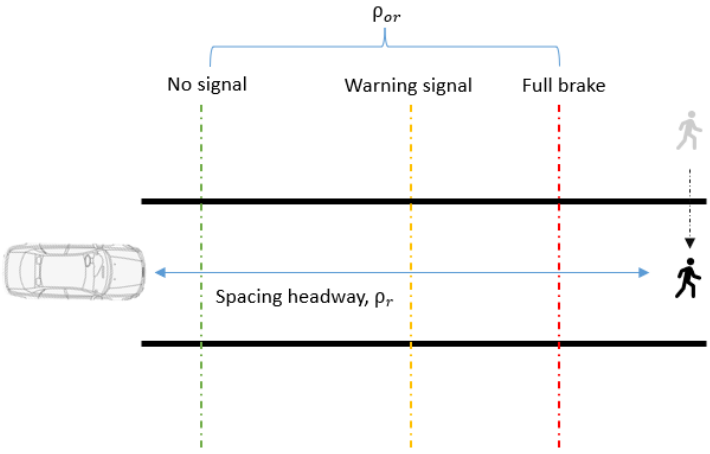

Figure 5. Activation phase of AEB-P system.

The deceleration of VC-APF, $\alpha_{VC\text{-}APF}$ can be obtained by deriving the Newton Second Law equation as follows:

$$\alpha_{VC\text{-}APF} = \frac{Frep(X)}{m} \tag{15}$$

The value of $\alpha_{VC\text{-}APF}$ will be compared with the desired deceleration in the vehicle dynamic control module, as in Figure 1. In the simulation, the desired deceleration is set to 8 m/s^2.

Vehicle Dynamic Control

After the redefined collision avoidance path has emerged, the vehicle dynamics control will track the path from the motion planning module. If the vehicle requires braking intervention to stop at a given distance and a pedestrian appears in front of the vehicle, a system with a short response time is preferred. This system is a simple and linear tracking system known as single-input and single-output (SISO), using deceleration and velocity of the vehicle as input and output, accordingly [8]. In this system, the vehicle dynamic control is handled by a PI controller. As it has its own abilities, the PI formulation variable refers to proportional and integral. As illustrated in Figure 6, the deceleration error is the difference between the required deceleration and the deceleration produced by the VC-APF path planner.

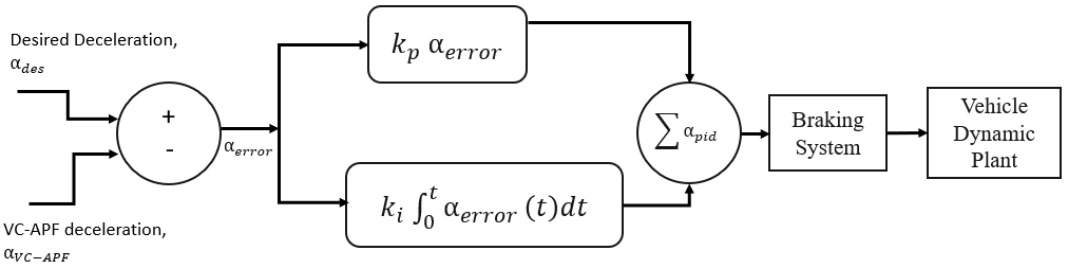

Figure 6. Block diagram of PI controller.

The ability of proportional gain is to boost the vehicle's deceleration response speed. If the proportionate gain is too great, the reaction will become shaky. Since it can integrate the error over time, the integrative variable can converge the steady-state error to zero. The tuning of the P and PI controller is based on the vehicle's constant desired deceleration of 8 m/s^2 [14]. The deceleration error, α_{error} between the desired deceleration, α_{des} and VC-APF deceleration, α_{VC-APF} is denoted as in Eq. (16). The PI controller equation can be expressed in Eq. (17) where α_{pid} is the desired trajectory deceleration, while K_p and K_i is the proportional and integral gain accordingly.

$$\alpha_{error} = \alpha_k - \alpha_{APF} \tag{16}$$

$$\alpha_{pid} = K_p\, \alpha_{error}(t) + K_i \int_0^t \alpha_{error}(t)\, dt \tag{17}$$

Table 2 below shows the P and PI controller variables as the vehicle is simulated on a dry road surface at different values of brake disc friction coefficients; 0.4, 0.35 and 0.24.

Table 2. PI controller variables on dry road surface.

μ_{disc}	Kp	Ki
0.4	0.88	0.0039
0.35	1.01	0.0026
0.24	1.48	0.0005

Braking System of AEB-P

The AEB-P system uses this disc brake system as an actuator. The coefficient of friction at the brake disc pad has a direct impact on the braking system's performance. The contact patch between the brake pad and disc rotor is shown in Figure 7.

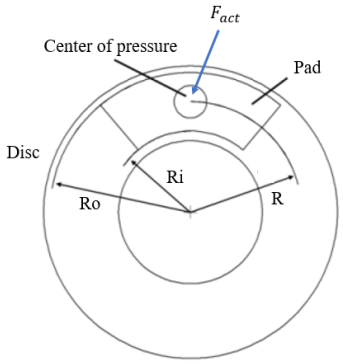

Figure 7. Contact patch between brake pad and disc rotor [20].

When a driver presses a brake pedal, the pedal braking force will be transferred to the brake calliper. The brake calliper's piston pushes the brake pad against the disc rotor, decreasing and subsequently stopping the wheel's rotation. The braking torque, T_b, is formed by multiplying the actuating force acting on the centre of pressure with the effective radius, F_{act} and R. The F_{clamp} is referred to as the force that clamped the disc brake. The actuation forces on disc brakes have pressed the piston against the rotor, resulting in disc brake retarding torque. $F_{friction}$ is stand for frictional force after the actuation force operating on it, $F_{friction}$ occurred at the disc brake.

$$F_{act} = m\alpha_{pid} \tag{18}$$

$$F_{clamp} = 2F_{act} \tag{19}$$

$$F_{friction} = \mu F_{clamp} \tag{20}$$

$$T_b = F_{friction}R \tag{21}$$

The braking torque on disc brakes can be written as in Eq. (22). F_{act} is obtained from the production of deceleration after P or PI controller tuning with the mass of the vehicle.

$$T_b = 2\mu_{disc}F_{act}R \tag{22}$$

The value of the brake pad's coefficient of friction, which is a disc, is varied in this simulation to explore the influence of the brake pad. The brake pad's coefficient of friction values of 0.4, 0.35, and 0.24 are used in the simulation.

RESULTS AND DISCUSSION

The results are based on the proposed AEB-P architecture, which starts with the pedestrian prediction module, which consists of the time-to-collision (TTC) and AEB-P activation phase. Then, the proposed method VC-APF in the motion planning and decision-making module are discussed with the consideration of the different brake disc pad friction coefficient for the dry road surface.

Pedestrian Prediction Module

Figure 8 shows the time-to-collision (TTC) and AEB-P activation system when a vehicle is driving on a dry surface. Based on Figure 8(a), the TTC can be used to establish whether there is a high danger of collision for pedestrians. The blue and purple color lines represented the host vehicle's time to collision and the time taken to count the pedestrian entering and exiting the collision region. The time for the pedestrian to escape and enter the collision area was depicted by the yellow and red color lines, respectively. When the pedestrian prediction module forecasts that the pedestrian is in the collision area, it begins to feed the VC-APF path planner the value of the vehicle's maximum safe distance from the pedestrian. Figure 8(b) shows when the car approaches the pedestrian, the AEB-P mechanism activates. The vehicle's spacing headway, warning signal phase, and full braking phase are shown by the blue, yellow, and red lines, respectively. As the vehicle's spacing headway crosses the warning signal phase, the warning signal begins to trigger at time 2.125 s. When the spacing headway passes the full brake phase at 3.7853 s, the AEB-P system applies an emergency brake. Because the pedestrian is expected to enter the collision area at 2.125 s, the value for full braking and warning signal phase increased suddenly at 2.125 s, as shown in Figure 8(a) and 8(b).

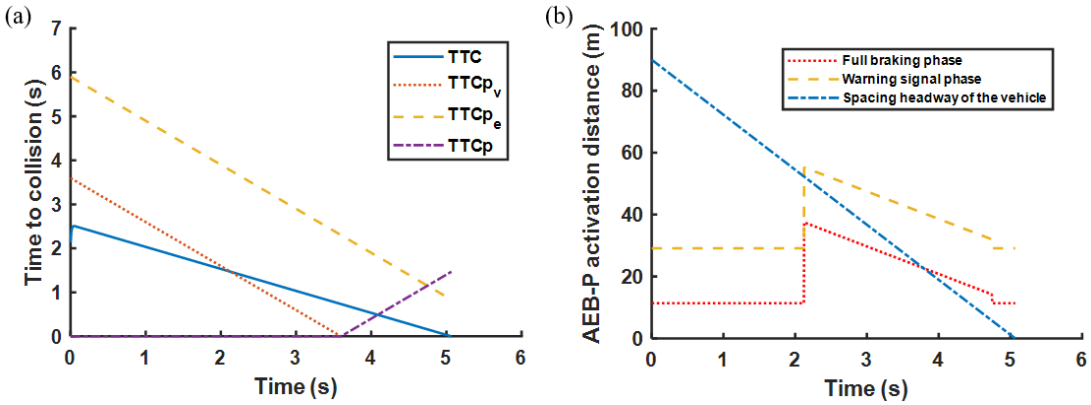

(a) Time to collision for the host vehicle (b) AEB-P activation distance

Figure 8. (a) The time-to-collision (TTC), (b) AEB-P system during braking on a dry surface.

Motion Planning and Decision Making

The performance of the motion planning and control is analyzed on varies brake disc pad friction coefficient, μ_{disc} = 0.4, 0.35 and 0.24 on dry surface conditions. After the pedestrian prediction module predicts the collision will occur, VC-APF path planner will send the warning signal to driver. If there is no response by the driver, the system will override the vehicle by generating the deceleration to the brake control unit. For getting the full braking force during emergency braking, the desired deceleration in the brake control unit is set at 8 m/s^2. In the brake control unit, the PI controller is used to obtain the desired deceleration, 8 m/s^2.

Figure 9 shows the behaviors of the VC-APF deceleration on dry road surface condition for different brake pad coefficient. Based on the equation deceleration of VC-APF, as in Eq. (15), an increase in the deceleration's value is influenced by the repulsive force, $F_{rep}(X)$. In addition, the $F_{rep}(X)$ will generate the warning signal and emergency braking when the distance between the host vehicle and pedestrian complies with the condition as in Eq. (12) and Eq. (13). The VC-APF motion planning start to initiate the deceleration at 3.7853 s which is 22.78 m from the pedestrian. Figure 9(a), 9(b) and 9(c) shows the deceleration value trend tends to increase smoothly and stop until it achieves maximum deceleration which is 6.617×10^{-5}, 6.201×10^{-5} and 5.784×10^{-5} for μ_{disc} = 0.4, μ_{disc} = 0.35, μ_{disc} = 0.24 respectively. These results show that the maximum deceleration generated by the VC-APF is too small compared with the desired deceleration, 8 m/s^2. The P and PI controllers are used in the braking control unit to minimize and eliminate the error between the acceleration VC-APF and desired deceleration.

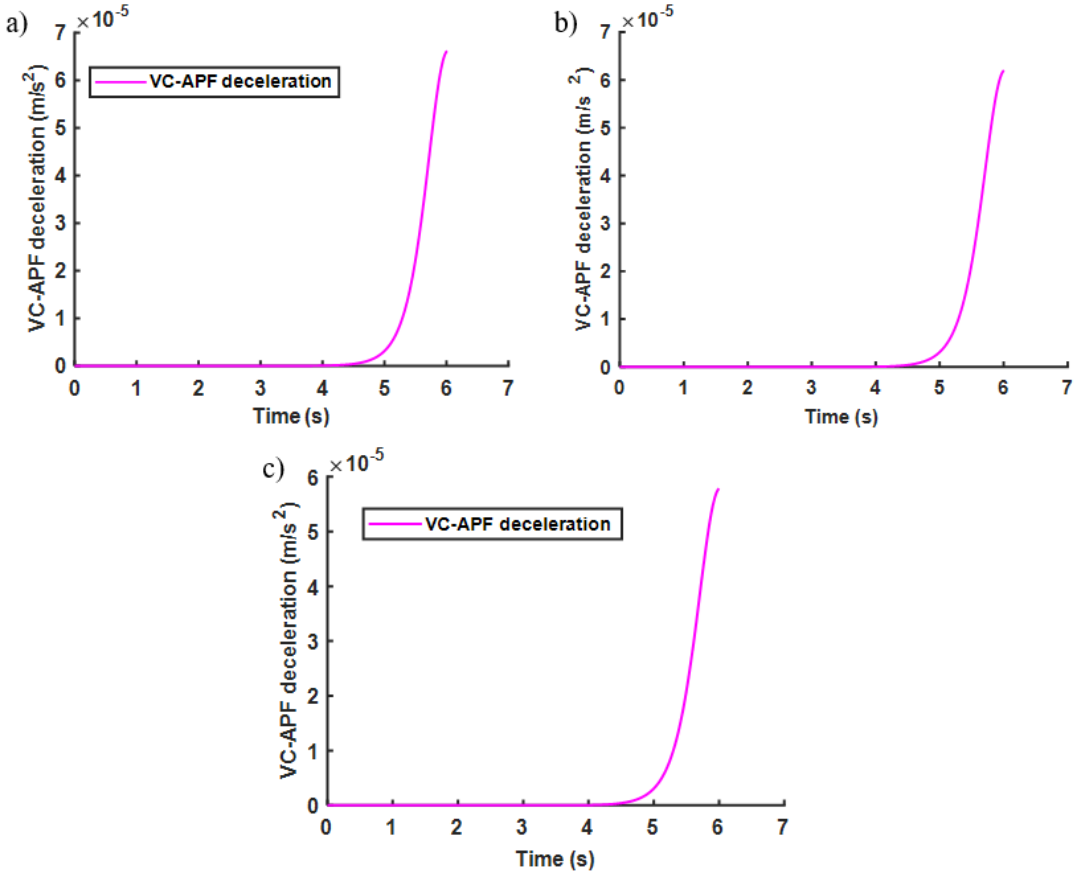

Figure 9. The behavior of the VC-APF deceleration on a dry road surface (a) μ_{disc} = 0.4, (b) μ_{disc} = 0.35 and (c) μ_{disc} = 0.24.

Braking Control Unit

The P and PI controllers are compared for different brake pad coefficients. Figure 10(a), 10(b) and 10(c) show the comparison of P and the PI controller for each brake pad coefficient. The analysis of the P and PI controller performance are summarized in Table 3.

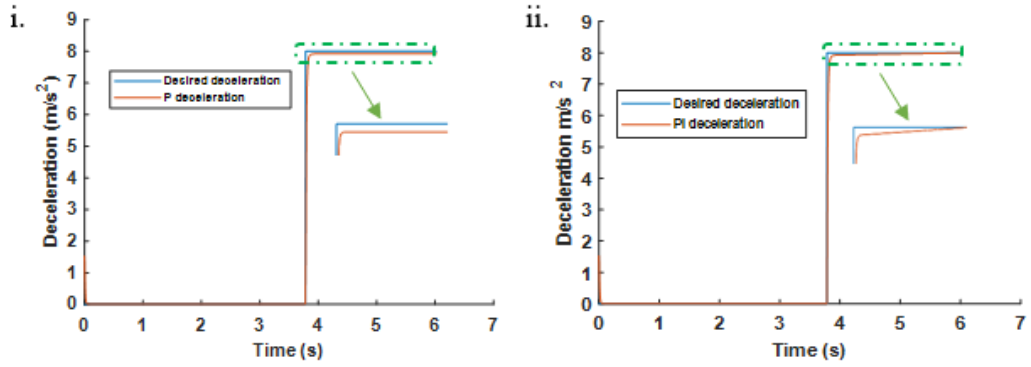

(a) Brake pad coefficient 0.4

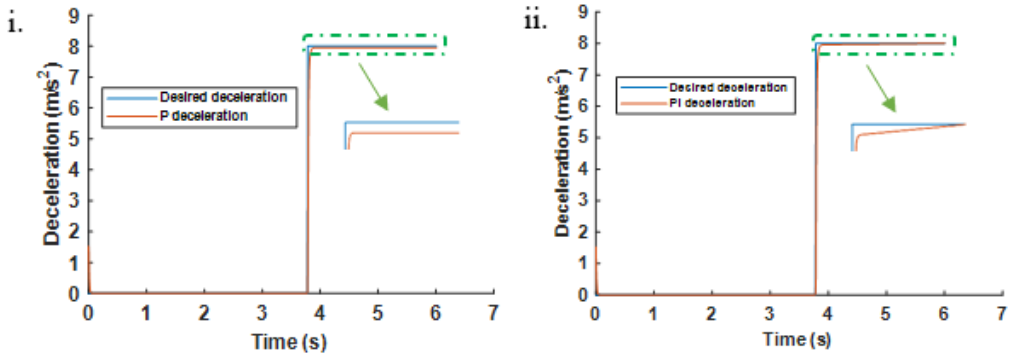

(b) Brake pad coefficient 0.35

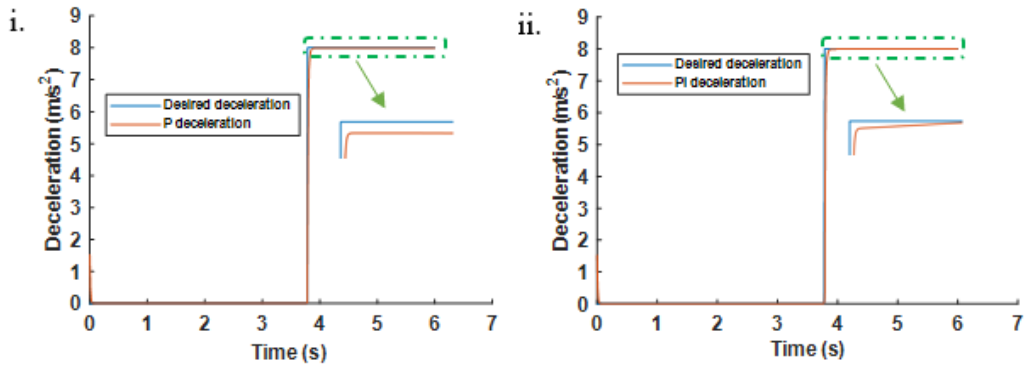

(c) Brake pad coefficient 0.24

Figure 10. The effect of P and PI controller during activation of AEB-P.

Table 3. P and PI controller response on a dry road surface.

μ_{disc}	Rise time (s)		Steady-state error	
	P Controller	PI Controller	P Controller	PI Controller
0.4	0.023615	0.024752	0.08011	0.00145
0.35	0.02367	0.024319	0.04610	0.0003061
0.24	0.023734	0.023817	0.007541	0.001516

The system rise time to reach the setpoint is fast for P controller compared to PI controller. However, the PI controller managed to reduce the steady-state error in this system compared to the P controller in Figure 10 above shows the ability of the integral, I variable in PI controller to reduce the steady-state error compared to the P controller. In terms of deceleration performance, the PI controller is slightly better compared to the P controller. Figure 10(a) shows the vehicle maximum trajectory deceleration in the PI controller managed to reach 7.999 m/s^2 compared to the P controller, which is 7.92 m/s^2. Figure 10(b) and 10(c) shows the vehicle maximum deceleration in P controller which is 7.954 m/s^2 and 7.993 m/s^2 respectively while in PI controller is 8 m/s^2 for μ_{disc} = 0.35 and 0.24. Figure 11(a), 11(b) and 11(c) show the dynamics behavior of the vehicle when simulated on a dry road surface at varied brake disc pad friction coefficient μ_{disc} = 0.4, 0.35 and 0.24, respectively.

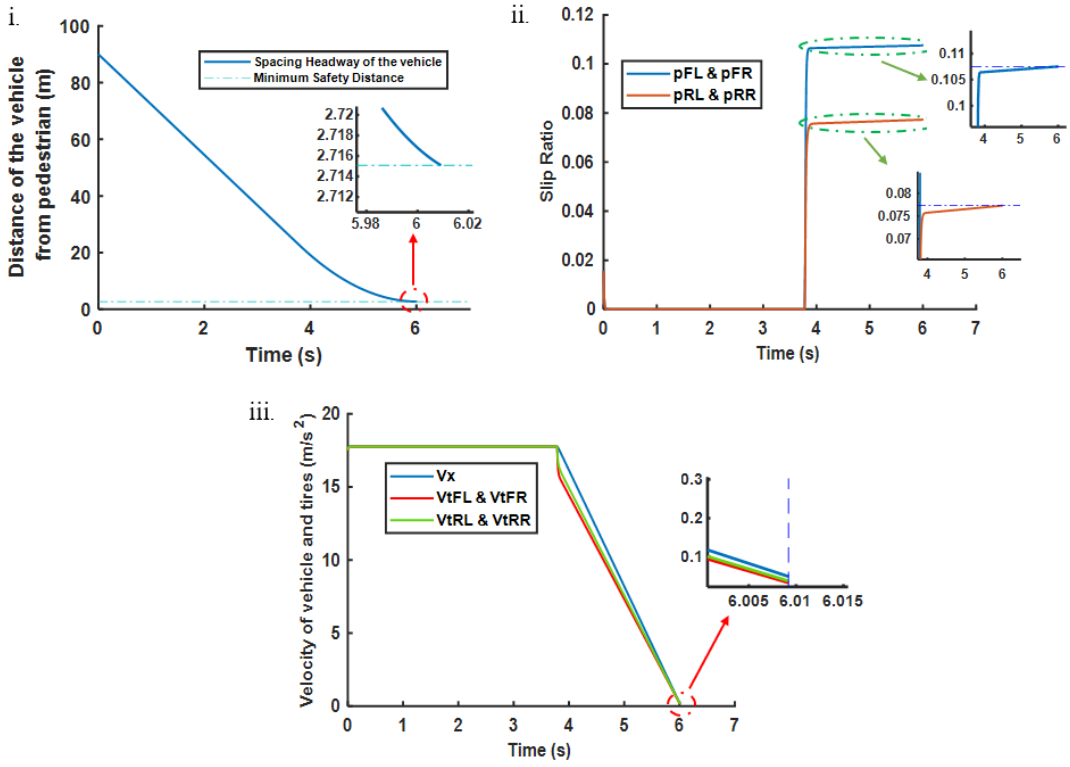

(a) Brake pad coefficient 0.4

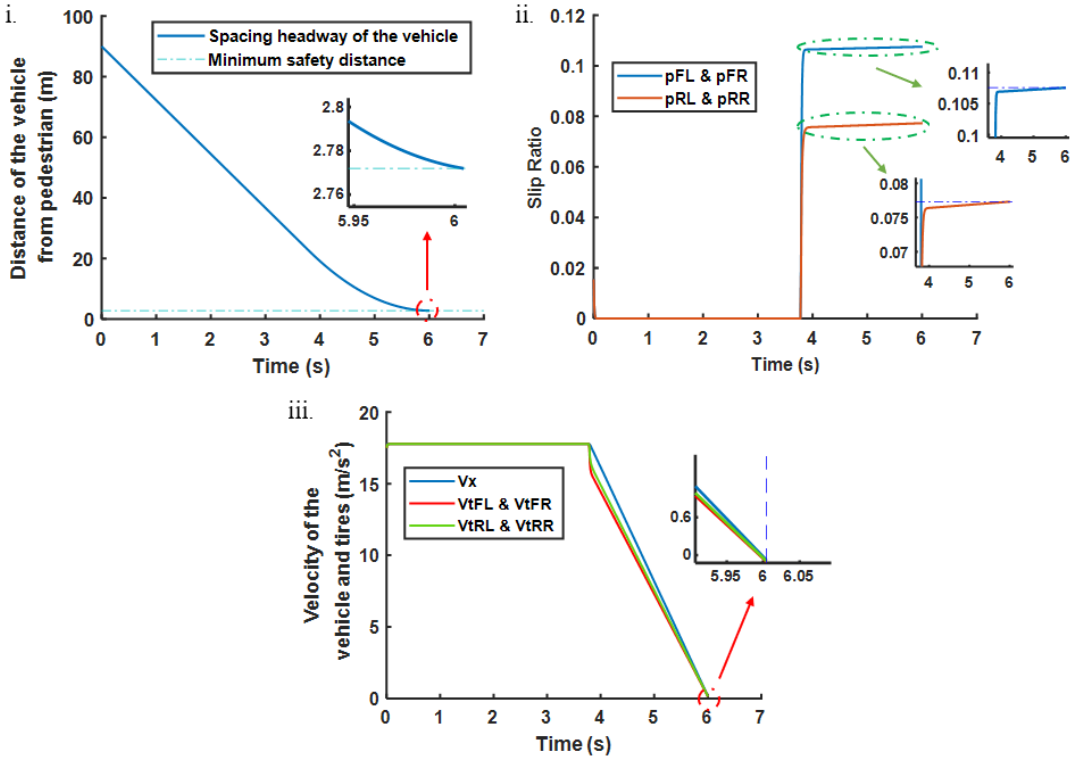

(b) Brake pad coefficient 0.35

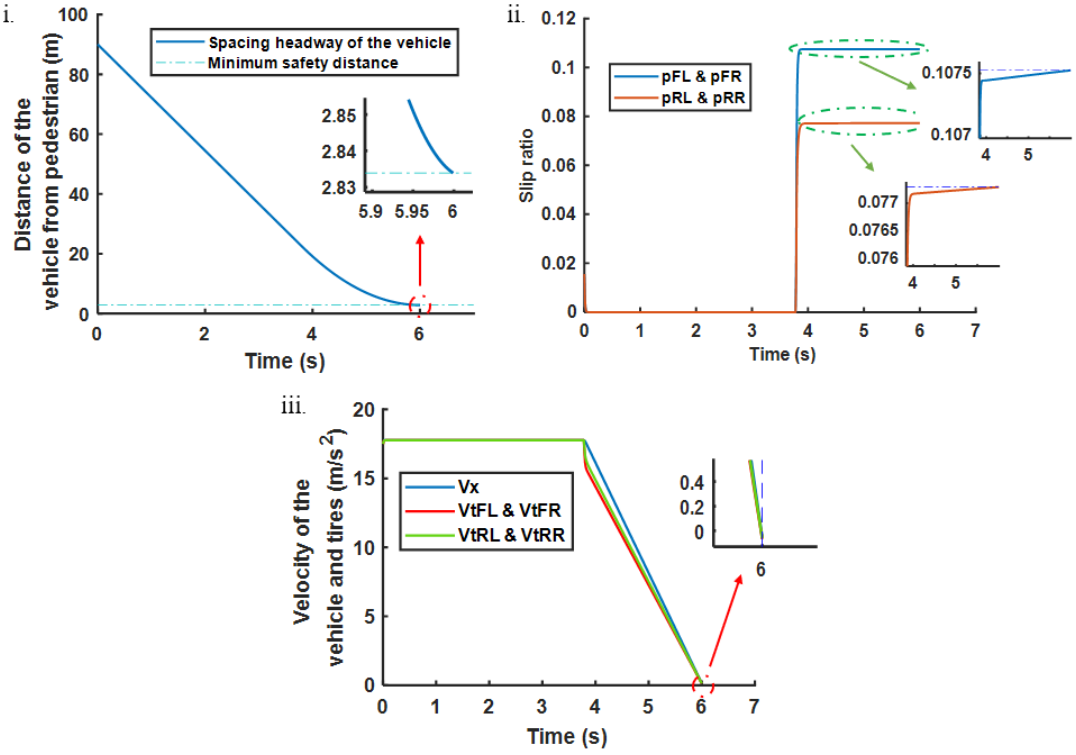

(c) Brake pad coefficient 0.24

Figure 11. Vehicle dynamics behavior for PI control response.

Each subfigure: i, ii and iii stands for the minimum safety distance of the vehicle, slip ratio of the tires as well as stopping time for the vehicle to stop, respectively. In this simulation, the PI controller is selected as a braking control unit to obtain the optimum deceleration for the brake actuator. Based on the spacing headway results as in Figure 11(a)i, 11(b)i, and 11(c)i, the vehicle is stopped before the minimum safety distance. This proved that the proposed AEB-P with PI controller could prevent the collision between vehicle and pedestrian, although the brake pad coefficient is low. The summary of minimum safety distance, maximum slip ratio and stopping time for all brake pad coefficients, as in Table 4.

From Table 4. , the vehicle manages to have a safety distance from the pedestrian in the range from 2.7 m to 2.9 m after executed an emergency braking when simulated at different brake disc pad friction coefficient. The higher deceleration of the vehicle will produce a longer minimum safety distance of the vehicle. The slip ratio of the front and

rear part of the tires is in the optimal slip ratio range during emergency braking. It is important to make sure the slip ratio is in the range of $0.075 \leq p \leq 0.211$ in order to avoid skidding phenomena. The slip ratio of each tires tends to increase directly proportional over time due to effect of integral variable in PI controller as shown in Figure 11(a), 11(b) and 11(c) for subfigure ii. The vehicle only takes below than 2.3 s to stop entirely when simulated on dry road surface for μ_{disc} = 0.4, 0.35 and 0.24.

Table 4. Vehicle dynamic behavior on a dry road surface.

μ_{disc}	Minimum safety distance (m)	Maximum slip ratio		Stopping time (s)
		ρ_{FL}, ρ_{FR}	ρ_{RL}, ρ_{RR}	
0.4	2.715	0.1075	0.07729	2.2247
0.35	2.772	0.1075	0.07729	2.2187
0.24	2.834	0.1075	0.07729	2.2137

CONCLUSION

In this study, a simulation model of VC-APF motion planner and PI tracking trajectory control has been developed to keep the minimum safety distance of the vehicle from pedestrian skidding while braking on the dry road surface with various brake disc pads friction coefficients. VC-APF is a reliable motion planner during emergency braking as it provides a warning signal and emergency braking phase distance for the host vehicle. The combination of VC-APF with PI controller is critical during braking because it can increase the VC-APF deceleration value approaching the desired deceleration that has been set. The vehicle manages to have a comfortable minimum safety distance which is in the range of 2.7-2.9 metres for various brake disc pad friction coefficients after emergency braking compared to the previous study [24], as the safety distance is set to 2.0 metres. These results approved that the proposed model, VC-APF and PI controller can increase the braking performance and safety of the vehicle. For future study, the consideration of wet road surfaces and integration between ABS and VC-APF is recommended to ensure the robustness of the VC-APF at the different road surfaces.

ACKNOWLEDGEMENT

The authors would like to thank University Malaysia Pahang (www.ump.edu.my) for providing an internal Flagship Grant under project number RDU192219. Special thanks to Automotive Engineering Centre, Universiti Malaysia Pahang and Intelligent Robotics and Vehicle (IROV) team members for providing technical support for this research.

REFERENCES

[1] M. Baharuddin, N. Khamis, K. A. Kassim, and M. Mansor, "Autonomous emergency brake (AEB) for pedestrian for ASEAN NCAP safety rating consideration: A Review," *Journal of the Society of Automotive Engineers Malaysia,* vol. 3, no. 1, pp.63-73, 2019.

[2] K. Hojjati-Emami, B. Dhillon, and K. Jenab, "Reliability prediction for the vehicles equipped with advanced driver assistance systems (ADAS) and passive safety systems (PSS)," *Int. J. Ind. Eng. Comput.,* vol. 3, no. 5, pp. 731-742, 2012, doi: 10.5267/j.ijiec.2012.08.004.

[3] S. M. Syazwan *et al.*, "Prevalence of distracted pedestrians while crossing: A study of Malaysia's situation," in *MATEC Web of Conferences*, 2017, vol. 90, p. 01031.

[4] T. Peng *et al.*, "A new safe lane-change trajectory model and collision avoidance control method for automatic driving vehicles," (in English), *Expert Syst. Appl.,* vol. 141, p. 112953, 2020,doi: 10.1016/j.eswa.2019.112953.

[5] M. Lin, J. Yoon, and K. Byeongwoo, "Proposal and verification of an AEB system algorithm based on slope and surface condition of roads," (in English), *Int. J. Appl. Eng. Res.,* vol. 10, no. 19, pp. 40109-40113, 2015.

[6] M. Rizzi, A. Kullgren, and C. Tingvall, "Injury crash reduction of low-speed Autonomous Emergency Braking (AEB) on passenger cars," in *Proc. of IRCOBI Conference on Biomechanics of Impacts*, 2014, pp. 14-73.

[7] M. Davidekova and M. Gregus, "Nice, Berlin, London - if every car had autonomous emergency braking system for forward collisions avoidance," (in English), In 14th International Conference on Mobile Systems and Pervasive Computing (Mobispc 2017) / 12th International Conference on Future Networks and Communications (Fnc 2017) / Affiliated Workshops, 2017, pp. 386-393,.

[8] U. Z. Abdul Hamid *et al.*, "Modular design of artificial potential field and nonlinear model predictive control for a vehicle collision avoidance system with move blocking strategy," (in English), *Proc. Inst. Mech. Eng. D: Journal of Automobile Engineering,* vol. 232, no. 10, pp. 1353-1373, 2018.

[9] U. Z. A. Hamid, H. Zamzuri, M. A. A. Rahman, and W. J. Yahya, "A safe-distance based threat assessment with geometrical based steering control for vehicle collision avoidance," *J. Telecommun. Electron. Comput. Eng. (JTEC),* vol. 8, no. 2, pp. 53-58, 2016.

[10] O. M. Ulises Orozco-Rosas, Roberto Sepúlveda, "Mobile robot path planning using membrane evolutionary artificial potential field," *Appl. Soft Comput.,* vol. 77, pp. 236-251, 2019, doi: 10.1016/j.asoc.2019.01.036.

[11] E. Bauer *et al.*, *Proreta 3: An integrated approach to collision avoidance and vehicle automation*, *Automatisierungstechnik Journal*, vol. 60, no.12, pp. 755-765, 2012.

[12] H. Hongyu, Z. Chi, S. Yuhuan, Z. Bin, and G. Fei, "An improved artificial potential field model considering vehicle velocity for autonomous driving," *IFAC-PapersOnLine,* vol. 51, no. 31, pp. 863-867, 2018.

[13] P. Raksincharoensak, T. Hasegawa, and M. Nagai, "Motion planning and control of autonomous driving intelligence system based on risk potential optimization framework," *Int. J. Automot. Eng.,* vol. 7, no. AVEC14, pp. 53-60, 2016, doi: 10.20485/jsaeijae.7.AVEC14_53.

[14] M. C. Mustafar and S. A. Bakar, "Optimal design of an Autonomous Emergency Braking (AEB) system for a passenger vehicle," in *IOP Conf. Ser.: Mater. Sci. Eng.*, vol. 884, no. 1, p. 012088, 2020, doi: 10.1088/1757-899X/884/1/012088.

[15] S. Bharat, A. Ganguly, R. Chatterjee, B. Basak, D. K. Sheet, and A. Ganguly, "A Review on Tuning Methods for PID Controller," *Asian J. Converg. Technol., (AJCT),* vol.5, no. 1, pp. 1-4, 2019.

[16] E. Joseph and O. Olaiya, "Cohen-coon PID tuning method; A better option to Ziegler Nichols-PID tuning method," *Engineering Research,* vol. 2, no. 11, pp. 141-145, 2017.

[17] P. Neis *et al.*, "Towards a better understanding of the structures existing on the surface of brake pads," *Tribol. Int.,* vol. 105, pp. 135-147, 2017, doi: 10.1016/j.triboint.2016.09.033.

[18] O. Towoju, "Braking pattern impact on brake fade in an automobile brake system," *J Eng. Sci.,* vol. 6, no.2, pp 11-16, 2019.

[19] M. Kchaou, A. Sellami, R. Elleuch, and H. Singh, "Friction characteristics of a brake friction material under different braking conditions," *Mater. Des.,* vol. 52, pp. 533-540, 2013, doi: 10.1016/j.matdes.2013.05.015.

[20] I. Zulhilmi *et al.*, "Investigation on vehicle dynamic behaviour during emergency braking at different speed," *Int. J. Automot. Eng.,* vol. 16, no. 1, pp. 6161-6172, 2019, doi: 10.15282/ijame.16.1.2019.6.0468.

[21] I. C. Han, B. C. Luan, and F. C. Hsieh, "Development of autonomous emergency braking control system based on road friction," In *2014 IEEE International Conference on Automation Science and Engineering, CASE 2014*, 2014, vol. 2014-January, pp. 933-937.

[22] W. Yang, X. Zhang, Q. Lei, and X. Cheng, "Research on longitudinal active collision avoidance of autonomous emergency braking pedestrian system (AEB-P)," (in English), *Sensors (Switzerland),* vol. 19, no. 21, p. 4671, 2019.

[23] H. K. Lee, S. G. Shin, and D. S. Kwon, "Design of emergency braking algorithm for pedestrian protection based on multi-sensor fusion," (in English), *Int. J. Automot. Technol.,* vol. 18, no. 6, pp. 1067-1076, 2017, doi: 10.1007/s12239-017-0104-7.

[24] W. Zhou *et al.*, "Developing an improved automatic preventive braking system based on safety-critical car-following events from naturalistic driving study data," *Accid Anal Prev*, vol. 178, p. 106834, Dec. 2022, doi: 10.1016/J.AAP.2022.106834.